

18 experimental results and provides recommendations for the tensile characterization of FRCM
19 materials.

20

21 **Key words:** Fabric reinforced cementitious matrix; Material behavior; Repair; Strengthening;
22 Tensile characterization; Test procedure.

23

24 **Introduction**

25 Fabric Reinforced Cementitious Matrix (FRCM) composites consist of one or more layers of
26 dry-fiber fabric reinforcement embedded in an inorganic matrix made of a cementitious or lime
27 based mortar enriched with a low dosage of short fibers and additives. They can be considered as
28 a subset of Textile Reinforced Concrete (TRC) composites that are intended specifically for
29 repair and strengthening applications and in which the fabric must be composed of dry-fibers,
30 meaning they are not completely impregnated by a resin. Both TRC and FRCM are part of a
31 larger family of brittle matrix composites (ACI 549 2013) which among others include normal
32 and high performing Fiber Reinforced Concrete (FRC) and Ferrocement (Arboleda 2014).

33 Given the increased interest in the utilization of FRCM composite systems for structural
34 retrofitting applications, their specifications need to be available. System specifications include
35 both material performance properties and installation instructions. While the manufacturer
36 determines the installation instructions, research laboratories determine the material properties
37 through experimental and analytical investigations. FRCM is a relatively new composite with
38 unique and complex behavior, yet proven performance as a structural strengthening technique
39 (Papanicolaou et al. 2008, D'Ambrisi et al. 2012, Ombres 2012, Babaeidarabad et al. 2014,
40 Loreto et al. 2014). FRCM strengthening systems present some advantages when compared with
41 Fiber Reinforced Polymer (FRP) materials, in particular when used for the reinforcement of
42 historical buildings as the matrix, consisting of an inorganic mortar, provides a higher
43 compatibility with the substrate and vapor permeability. The complexity of FRCM behavior has
44 given rise to numerous research studies on the aspects that influence its mechanical properties.

45 The aim of this paper is to provide a context and recommendations for the determination of the

46 test method to be used to characterize the tensile behavior of FRCM composites based on the
47 type of parameters sought.

48 ***Overview of Tensile Test Methods for FRCM***

49 For structural reinforcement design, the values of the mechanical and bonding properties of the
50 applied materials must be known. These values are determined through experimental tests. The
51 apparent uniaxial tensile behavior of this type of composite is influenced by several factors
52 including the load transfer mechanism (grip method), specimen geometry and fabrication, and
53 strain measurement technique. Since none of these factors are yet standardized, various set-ups
54 for FRCM tensile tests with different gripping methods and specimen geometries have been
55 developed (Contamine et al. 2011, Zhu et al. 2011, Hartig et al. 2012, Arboleda et al. 2012).
56 Figure 1 shows the main gripping methods used by different research groups. Hartig et al. (2010)
57 identified two types of load application: “rigid load application” (Figure 1a and 1c) in which the
58 transfer mechanism between the specimen and the grip is by adhesive tension and shear realized
59 through metal plates glued to the specimen ends (in this study realized with “clevis grip”), and
60 “soft clamping” (Figure 1d) which uses friction for load application realized by applying a
61 compressive force normal to the plane of the specimen at its ends.

62 Molter (2005) proposed a waisted specimen in which the mortar is prevented from cracking
63 within the supported range. Steel plates are glued or inserted inside the specimen, causing the
64 load transfer mechanism between specimen and clamping through adhesive tension and shear,
65 and no slip can occur between clamping and specimen (Figure 1a). The clamps adopted for bone-
66 shaped specimens (Figure 1b) are articulated steel flanges located in the curved part of the
67 specimens over a rubber sheet (Orlowsky and Raupach 2008). The ICC-Evaluation Service
68 acceptance criteria (AC434 2013) recommends gripping the specimen through adhesive tension

69 and shear method such as a clevis grip (Figure 1c). This includes two plates glued at each end of
70 the specimen and connected with a transversal pin outside of the length of the specimen. This
71 system is connected with a clevis joint to the testing frame.

72 Other research groups (Carozzi et al. 2015, De Santis et al. 2015) proposed an alternative system
73 in which the two extremes of the specimens are fixed into the grips of a standard testing machine
74 but the lower grip allows for torsional rotation. In this case the clamps produce compressive
75 stresses at the end of the specimens where fiber reinforced tabs are applied using epoxy resin in
76 order to facilitate a more homogeneous stress distribution and avoid local damage in the matrix.

77 In reference to specimen geometry, rectangular shaped FRCM coupons are generally easier to
78 implement and fabricate than waisted ones such as the dumbbell (Hegger et al. 2006), for which
79 the specimen section is gradually increased at its ends and a perforated metal plate is placed at
80 mid-thickness to ensure the transmission of force. A variation of the dumbbell was used by
81 Papantoniou and Papanicolaou (2012) in which the specimen's end sections are thicker than the
82 rest of the specimen. Other types of waisted specimens include bone-shaped specimens (Raupach
83 et al. 2006), which require expensive molds and particular care in implementation. Rectangular
84 shaped specimens are often cut from larger panels which tend to provide more control of
85 production, but can also be made from single molds requiring more careful manufacture to
86 ensure proper alignment of the fabric. The rectangular shape is recommended as it ensures the
87 integrity of the rectangular geometry of the fabric.

88 Different procedures to measure the deformation are available. Roth (2007) used strain gauges
89 that provide locally accurate information, but are inadequate in case of multi-cracking behavior.

90 Clip-on and laser extensometers are reliable techniques which also allow for the determination of
91 possible misalignment of the specimen due to out-of-plane bending. Photogrammetry and digital

92 image analysis are other refined methods that provide a complete overview of the crack
93 formation in the specimen. These would be adequate systems of measurement but are sensitive to
94 loss of focus due to specimen curvature (Arboleda et al. 2013) and can become burdensome for
95 large series of tests due to extensive data analysis. AC434 (2013) suggests the use of “*an*
96 *extensometer with a minimum gauge length of 50 mm that shall be adequate to include at least*
97 *one significant crack*”.

98 **Overview of Tensile Behavior**

99 Typical stress-strain behavior of FRCM under tensile test (Figure 2b) is idealized as a tri-linear
100 curve (Jesse et al. 2008). The first linear phase represents the uncracked state of the composite
101 controlled by the matrix properties which are enhanced by the presence of fibers. The second
102 phase corresponds to the formation and propagation of cracks. In this state there is a significant
103 decrease of the stiffness and relatively fine cracks form. The length and slope of this portion of
104 the curve depend on the quality of the bond between fabric and matrix and on the volume
105 proportion of the fibers activated for load transfer (Butler et al. 2010).

106 The third phase is the crack-widening region, where the existing cracks become wider up to the
107 final failure caused either by reaching the tensile strength of the fabric, or by slippage of the
108 fabric from the matrix, or a combination of both. This phase is defined by a number of factors
109 including end boundary conditions and fabric properties such as volume percent, geometry, and
110 whether the yarns are fully impregnated by resin or dry, meaning only partially impregnated by
111 the cementitious matrix or yarn partially coated by resin thus having a dry fiber core held in
112 place only by frictional forces. In this phase only the fabric resists the load and, therefore, the
113 slope of the curve often reflects the elastic modulus of the dry fibers. In certain conditions a
114 tension stiffening effect is observed where the modulus in this phase runs parallel, but at a

115 slightly elevated stress compared to the fabric (Figure 2b). This is attributed to a contribution of
116 the uncracked matrix between the cracks. In conditions where the matrix strength is very low or
117 the dry fibers slip, the modulus of the third phase can be undistinguishable from the second
118 phase and a bi-linear behavior is obtained instead (Figure 2c).

119 The transition points T_1 and T_2 are defined at the change in slope of the stress-strain curve and
120 are determined by the intersection of the linear portion representing the modulus of elasticity of
121 each phase. Furthermore, cementitious composites with insufficient fabric volume will behave as
122 FRC with strain softening and are not considered FRCM composites.

123 ***Fiber to Matrix Bonding***

124 When yarns are fully impregnated with resin they behave as internal FRP and increase the
125 organic content of the composite. By definition, FRCM is composed of “dry-fiber fabric”,
126 meaning that the yarns are not fully impregnated with resin. When the fabric is completely dry,
127 the mortar partially impregnates the outer fibers in the yarn bundle. When the fabric has a
128 protective coating applied on the exterior of the yarn the mortar does not impregnate the bundle.
129 In either case, however, there is a core of dry fibers. Therefore dry fiber yarns can be modeled as
130 having a sleeve and a core. It is important to investigate the adhesive bond between the external
131 fibers of the yarn and the mortar and also the frictional bond among the internal fibers within the
132 yarn.

133 Two types of slippage can occur: between fibers and mortar or within fibers in the dry core of the
134 yarn. Slippage between fibers and mortar is due to incomplete impregnation of the fibers,
135 debonding, or to chemical incompatibility, and can be localized at the end of the specimen or in
136 each crack region. Slippage appears between the fibers in the yarn due to a telescopic failure
137 mode. It is known that a cement matrix is not ideal to impregnate fibers. The external fibers in a

138 yarn are either in direct contact with the matrix or indirect contact with the matrix through the
139 partial protective coating and are thus tightly bonded, while the internal fibers in the core of the
140 yarn are not and can slip more easily because of the low friction between the fibers.

141 Peled (2008), Soranakom and Mobasher (2009) and Andic-Cakir (et al. 2014) presented a model
142 to simulate the yarn as a cylindrical structure comprised of concentric rings composed of several
143 fibers. The failure mode of the fibers in the sleeve is by fracture while the internal fibers slip due
144 to the pull-out force. The telescopic mode pull-out (Banholzer et al. 2006) is influenced by
145 cement penetrability, the geometry of the reinforcement, the presence of a coating, and the level
146 of friction between the fibers in each yarn.

147 **Experimental Program**

148 Rectangular coupons of various FRCM systems were tested using two different test setups. The
149 main difference between the set ups was the gripping method used to transfer the load. Since grip
150 terminology is not standardized, in this paper “clevis grip” is the term used for load application
151 through metal tabs glued on the specimen ends (Figure 1c) and "clamping grip" is the term used
152 for load application through compressive stress normal to the specimen's plane (Figure 1d). The
153 main difference between the two methods is the stress state generated by the grips. In the first
154 case, only shear stresses are transferred. In this type of test the full strength of the fabric is never
155 reached because the failure mode is by slippage of the fabric. In the second case, the clamping
156 grips generate compression and shear in the specimen to limit slippage between fabric and matrix
157 at the grip.

158 The tests performed with clamping grips allow a complete mechanical behavior characterization
159 of the composite with a tensile failure of each constituent material, however, in field applications

160 of FRCM the ends are not anchored and failure is often by slippage of the fibers. Thus the tests
161 performed with clevis grips intend to reproduce the as-installed FRCM behavior.

162 ***FRCM composites used during the investigation***

163 Five different FRCM systems were used during this study having these types of fabrics:

- 164 - polyparaphenylene benzobisoxazole (PBO fiber), composed of dry fibers only
165 (Figure 3a);
- 166 - two types of carbon (“C fiber” and “cC fiber”), one composed of dry fibers only
167 (Figure 3b), the second one having a protective coating over the dry fibers;
- 168 - two types of glass fabric (“G fiber” and “cG fiber”), the first one composed of dry fibers
169 only, the second one having a protective coating of Styrene Butadiene over the dry fibers.

170 Each type of fabric was matched with the mortar that is specifically designed for it by the FRCM
171 system manufacturer. The corresponding systems are denominated “x-FRCM”, where “x”
172 represents the name of the fabric (e.g.: “PBO-FRCM”).

173 ***Fabric reinforcement***

174 Figure 4 shows the geometry of the different fabrics involved in the experimental study. Fabric
175 parameters shown include spacing between yarns and yarn nominal width. For unbalanced
176 fabrics (different fiber volume in each direction) the warp (main or load carrying) direction is
177 shown up/down and the weft direction is shown left/right. Another important parameter is the
178 equivalent thickness, which is used to determine the nominal cross sectional area of the fabric
179 when multiplied times its length.

180 The “PBO” fiber unbalanced fabric has equivalent thickness in the warp and weft directions of
181 0.046 mm and 0.011 mm respectively. The carbon fiber (“C fiber”) is a balanced fabric with

182 equivalent thickness is 0.047 mm in both directions. The coated carbon fiber (“cC fiber”) is an
183 unbalanced fabric with equivalent thickness of the dry fibers in the warp direction of 0.175 mm.
184 The glass fiber (“G fiber”) balanced fabric has an equivalent thickness of 0.036 mm per direction
185 and the coated glass fiber (“cG fiber”) unbalanced fabric has an equivalent thickness of 0.05 mm
186 and a dry yarn net cross sectional area of 0.9 mm².

187 Tensile tests of single yarns and of fabric strips of width 40 and 50 mm (containing 3 to 4 yarns
188 as indicated in Table 1) in the warp direction were performed according to EN ISO 10618/2005
189 (2005). Tests were carried out using different testing machines with maximum load capacities of
190 2 kN and 100 kN and an extensometer with base length equal to 50 mm. In order to avoid local
191 damage during the tensile tests, special tabs of glass fiber reinforced polymer (GFRP) were
192 bonded using epoxy resin at the ends of the coupons. The tabs presented a width equal to the
193 coupon and a length equal to 60 mm.

194 The failure mode shows a rupture of some fibers without a complete failure of the yarn for PBO
195 and carbon fibers, in contrast a complete cut is evident in glass fibers. The failures occurred on
196 the length of the specimens, not close to the grips. Due to the difficulties of bonding all the
197 internal filaments in the tabs, it is very difficult to guarantee an homogeneous stress distribution
198 in the filaments of the yarn. For this reason all filaments don’t fail simultaneously. The
199 experimental results are summarized in Table 1.

200 ***Inorganic matrix***

201 The inorganic matrix is specifically designed by each manufacturer of the FRCM composite
202 system to a) provide optimal fresh state and workability properties, and b) form an optimal
203 (chemical/mechanical) bond with the fabric and the substrate. The constitutive components of
204 the mortar are not very different that traditional cement but some of the dry additives are

205 proprietary in nature and each fabric is used with its specific mortar. The matrices analyzed in
206 this work are cementitious mortars enriched with short fibers in a percentage less than 5%. Only
207 the mortar used with “G fibers” is lime based. Table 2 shows the main measurable mechanical
208 properties and the corresponding experimental standards adopted. Some of the values were
209 experimentally verified on mortar samples made and cured for 28 days in laboratory ambient
210 conditions of 20 °C and 60 % relative humidity, while others were taken from the technical data-
211 sheets provided by the producers. Some of the mechanical properties of the matrix were not
212 reported in the data-sheets. Reasonable values were estimated on the basis of a few tests.

213 ***Specimen geometry and preparation***

214 The test coupons were all rectangular and manufactured using a manual impregnation technique
215 in a flat rectangular mold by first applying a thin layer (5 mm) of the cementitious matrix,
216 followed by pressing a layer of the fabric into the mortar. The top layer of mortar matrix was
217 then applied as flat as possible with a finishing trowel. The cCarbon fabric had retained some
218 curvature from the roll it comes from and was placed in an oven at 60°C for 10 minutes the night
219 before so the coating could soften and the fabric sheet flattened out. All FRCM systems were
220 made with one fabric layer, but additionally, coupons were made with overlap splice for PBO
221 and carbon (PBO-FRCM and C-FRCM), and with two fabric layers for coated carbon
222 (cC-FRCM).

223 The fabricated panels were cured at laboratory ambient conditions at temperature 20°C and 60%
224 relative humidity for 28 days before cutting the individual coupons using a diamond-tipped wet
225 saw. The coupons tested with the clevis grip had nominal dimensions equal to 410 x 50 x 10 mm
226 and were cut from larger panels of 430 x 560 mm. The coupons tested with clamping grips were
227 made in a similar way, but each coupon was prepared in a flat mold separately.

228 **Test set-up**

229 ***Gripping***

230 Adhesive tension and shear grips were implemented with a clevis. Metal tabs of 3 mm thickness
231 with a bond length equal to 150 mm were fixed at the coupon ends with epoxy resin. The grip
232 had multiple degrees of freedom providing a pinned end support. This configuration reduces
233 bending moments and allows slippage of the fabric at the grip ends.

234 For complete mechanical characterization of the system clamping grips were selected. The two
235 extremes of the coupon were fixed into the grips of a standard testing machine, with the lower
236 grip allowing for torsional rotation thus ensuring specimen alignment prior to test start. In this
237 case the clamps can produce high compressive stresses (4-5 MPa) at the end of the coupons so
238 GFRP tabs (dimensions 60 x 40 x 2 mm) were applied using epoxy resin in order to avoid
239 damage in the matrix and guarantee an homogeneous stresses distribution.

240 ***Instrumentation***

241 For the tests performed with clevis grip, a test frame with a maximum capacity of 130 kN was
242 used with displacement control at a rate of 0.25 mm/min. Axial deformation was measured using
243 a clip-on extensometer with a 100 mm gauge length, placed mid-length of the coupon
244 (Figure 5a).

245 For the tests performed with clamping grip, a test frame with load capacity of 100 kN was used
246 with displacement control at a rate of 0.1 mm/min during the first phase (before matrix
247 cracking), and 0.3 mm/min thereafter. Deformation was measured using an extensometer with a
248 gauge length of 100 mm positioned in the central area of the coupon (Figure 5b). Since the
249 dimension of the coupon was 400 x 40 x 10 mm, the distance between the two grips of the

250 testing machine was 280 mm. Therefore the extensometer gauge length of 100 mm covered
251 about 1/3 of the free surface of the coupon giving an adequate measurement of the strain field.

252 ***Influence of different elongation measurements and gauge length***

253 Extensometers are installed on the external surface of the specimens and can provide only an
254 average deformation of the mortar matrix in the gauge length segments. The deformation through
255 the cross-section of the FRCM material is not homogeneous and difficult to measure. While the
256 mortar is brittle with a relatively high axial stiffness (AE) and low tensile strength, the fabric has
257 a lower axial stiffness and very high tensile strength. Additionally, the telescopic behavior of the
258 fabric yarns where the fibers experience internal frictional sliding cannot be measured with
259 classical strain measurement instruments installed on the exterior of the material.

260 The most common approach to FRCM strain measurement is with point-to-point instruments
261 such as extensometers and linear variable differential transformers (LVDT). With point-to-point,
262 location within the specimen width is important because the deformation can be different on each
263 side due to uneven crack widths. Thus, the measurements can be referred only to the midsection.
264 Furthermore, when any crack develops outside the instrument's gauge, the immediate response
265 measured by the instrument, can be of partial contraction. Particular attention in determining the
266 first transition point should be paid when the very first crack appears outside the instrument
267 gauge.

268 When the failure mode includes fiber debonding and slippage (Figure 6a), the instrument records
269 the slippage which occurs outside the gauge length. When slippage is prevented by clamping
270 grips, the strain in the fibers in the outer part of the bundles is equal to the strain experienced in
271 the matrix. Once the crack occurs, the fibers within the crack opening are then free to deform

272 according to their own properties. The length of the fibers that are free to deform is longer than
273 the crack width (Figure 6b).

274 Brittle matrix composites develop multiple cracks along the coupon length which form part of its
275 damage progression mechanics. The crack size and distribution within the coupon is a separate
276 measurement which cannot be captured with elongation measurement instruments. This
277 information, while not considered during application design, is part of the characteristic tensile
278 behavior of the composite and is often analyzed. Peled and Mobasher (2006) and Carozzi (2015)
279 studied the crack formation pattern. Peled and Mobasher (2006) determined that the crack
280 formation is a function of stress and fabric volume and are the primary mode of displacement.
281 Also that crack spacing diminished during loading and reached a steady state where no more
282 cracks appear calling this the point of crack saturation after which fiber debonding becomes the
283 secondary mode of displacement. Carozzi (2015) further determined that the spacing of cracks is
284 related to the fabric geometry, in particular, the spacing, width, and thickness of the weft yarns.

285 **Experimental results**

286 A variety of FRCM systems with one fabric layer were tested. Coupons with a layer splice
287 overlap (PBO and C-FRCM) and with two fabric layers (cC-FRCM) were also tested. Their
288 stress-strain behavior and failure modes were analyzed. A detailed description of the results
289 obtained can be found in (Arboleda 2014, Carozzi et al. 2015). In this paper the results are
290 summarized and critically analyzed to highlight the comparison of the two testing procedures. All
291 specimens demonstrated multiple cracking of the matrix, perpendicular to the direction of the
292 load, throughout the length of the coupon. The point at which no more cracks develop is termed
293 crack saturation.

294 For all specimens, the stress was determined by dividing the load by the nominal cross-section
295 area of the fabric only,³ because after the specimen starts to crack, the load transfer occurs
296 mainly through the fabric. Naturally, when the uncracked portion of the response curve is
297 determined using the actual cross-section of the specimen, the resulting first crack stress and
298 modulus of elasticity are comparable to that expected of the mortar only. Furthermore, since the
299 specimen cross-section has significantly more variability than the nominal fabric cross-section,
300 the high variability noticed in this first phase is reduced when first crack is based on gross area.

301 ***Clevis grip on one layer specimens***

302 The typical failure mode obtained with this test set up was slippage of the fabric within the
303 matrix after crack saturation. The fabric slippage is a combination of pull-out and tensile failure
304 of the fibers. The stress-strain behavior is bilinear with the first phase identified as the un-
305 cracked specimen behavior; when the first cracks appear the slope decreases and slippage
306 between fibers and mortar is eventually observed.

307 The modulus of the un-cracked specimen was calculated as the slope between the origin and the
308 intersection of the linear trend of the first portion of the experimental curve and the linear trend
309 of the second portion of the experimental curve. On the segment of the response curve
310 corresponding to cracked behavior after the transition, two points are selected at a stress level
311 equal to 0.90 f_{fu} and 0.60 f_{fu} (AC 549 2013). The slope of the line that connects these two points
312 represents the tensile modulus of elasticity at that region as summarized in equation (1):

$$313 \quad E_f = \frac{\Delta f}{\Delta \varepsilon} = \frac{0.9f_{fu} - 0.6f_{fu}}{\varepsilon_{@0.9f_{fu}} - \varepsilon_{@0.6f_{fu}}} \quad (1)$$

314 The segment between 0.90 f_{fu} and 0.60 f_{fu} was selected based on a statistical analysis of
315 representative curves in order to ensure consistency of results. Table 3 summarizes average

316 results with coefficient of variation and Figure 7 shows the tensile response of the different
317 FRCM materials. The G-FRCM and cG-FRCM were not tested with the clevis grip.

318 ***Clamping grip on one layer specimens***

319 With this gripping system, the typical failure mode is by damage to the fabric fibers close to the
320 main cracks. In a few instances, fiber slippage is observed and is attributed to poor bond to the
321 matrix. The stress strain behavior is predominantly tri-linear with exceptions based on the type of
322 FRCM material tested. Results show a large variability in the localization of transition points.
323 This is caused by a) the variability in dimensions of the specimen section; b) the presence of
324 cracks not visible to the naked-eye; and c) the location of the first crack with respect to the
325 extensometer (Bertolesi et al. 2014).

326 Tensile tests on C-FRCM and PBO-FRCM show a tri-linear behavior, G-FRCM and cG-FRCM
327 show a behavior where the second transition point is not evident due to the low elastic modulus
328 of the glass fibers. When the slope of the third branch is lower than the elastic modulus of the
329 dry fabric, a possible slippage phenomenon is occurring.

330 The modulus of all three phases is evaluated as the ratio between stress and strain of the first and
331 last point of each phase. For the first phase only, in which the mortar is un-cracked, tensile stress
332 (σ_{t1}^*) and elastic modulus (E_1^*) were also evaluated using the composite cross section in order to
333 compare the cracking tensile stress and the elastic modulus with the mortar properties. The stress
334 reached at the end of the first phase should be similar to the mortar tensile strength. As
335 previously described, due to possible problems in sample preparation or in the curing phase (no
336 planarity, different shrinkage, micro-cracking) this value could be lower than the mortar tensile
337 strength.

338 Table 3 summarizes average results with coefficient of variation and Figure 8 shows the tensile
339 response of four different FRCM materials (cC-FRCM not tested). The third phase shows most
340 of the differentiation due to the different elastic moduli and tensile strengths of the fibers.
341 Figure 9 and Figure 10 show the comparison between the stress-strain curves obtained with the
342 two gripping methods for PBO-FRCM and C-FRCM coupons. The characteristic behavior in the
343 first phase is not expected to be very different for both gripping methods, however, since the
344 stress is computed with respect to the textile cross-section area, the variable dimensions of the
345 cross section area of the matrix as well as the location of the first crack with respect to the gauge
346 length have a significant influence on the analyzed results. For tests performed with clevis grip
347 the second phase reached higher strain due to fiber slippage, and the third phase was not present.

348 ***Clevis grips on two layer specimens***

349 In order to analyze the efficiency of multiple layers, clevis grip tests were performed on coupons
350 with two layers of coated carbon (cC) fabric. Six tests were performed; Figure 11 and Table 3
351 show the stress-strain curves and the results summary. The failure mode was by slippage of the
352 fabric after crack saturation. The bi-linear behavior was observed consistent with one layer
353 coupons. A post failure phase showed increased “pseudo-ductility” due to the friction between
354 the two fabric layers and the mortar.

355 ***Clevis grips on splice specimens***

356 Investigation of fabric splicing with clevis grips showed that generally, the overlap length must
357 be greater than or equal to the tab length used for load application which itself is a function of
358 the fabric development length within the matrix. Preliminary results demonstrate that an overlap
359 of 100 mm is insufficient and must be increased to a minimum of 150 mm. In PBO-FRCM tests

360 the transition point occurs at a greater stress in the coupon with overlap due to the increase in
361 matrix thickness, after the cracking phase, the slippage phenomena develops between fabric and
362 mortar. Figure 12 compares the results for PBO-FRCM with the two gripping systems.

363 ***Clamping grips on spliced specimens***

364 Tensile tests were performed on coupons with a fabric overlap in the midsection to determine the
365 minimum overlap length. Two fabric layers were placed in the coupons, with a central splice
366 overlap of 100 mm. Six tests were performed on PBO-FRCM coupons, and five tests were
367 performed on C-FRCM. The fabric area was considered equal to one layer. The failure mode was
368 slippage of the fabric between the two layers from the coupon center, for this reason the slope of
369 the third phase and the maximum strength are lower than the one obtained with one layer
370 coupons. These results indicate that a length of overlap equal to 100 mm is not sufficient to
371 guarantee a proper stress transfer for the systems tested.

372 **Influence of different gripping methods**

373 As demonstrated by several studies (Contamine et al. 2011, Bianchi et al. 2013, Arboleda 2014,
374 Carozzi et al. 2015) , the resulting mechanical behavior for tensile tests is dependent on the
375 gripping at the ends of the coupon, specifically, trilinear for clamping grip, and bilinear for clevis
376 grip. This consideration must be clearly understood when defining a procedure to be used for
377 material characterization. Clearly, the maximum strength is the parameter wanted, but this is not
378 possible to achieve as installed.

379 When the goal of the characterization is to determine the maximum possible strength of the
380 composite, then clamping grips are necessary. However, when the goal of characterization is to
381 determine the parameters useful for design when the material is installed per manufacturer's

382 instructions (wet layup or spray), then a clevis grip that permits failure by slippage is required. It
383 is possible, however, for an installation to take place with anchoring of the material at the ends in
384 order to prevent the slippage phenomena in which case the maximum strength of the composite
385 could be the sought after design parameter.

386 **Contribution towards the development of a test protocol for characterization of** 387 **FRCM composites**

388 On the basis of the series of experiments performed, the following steps are proposed as part of a
389 testing procedure for characterization of FRCM coupons in tension:

390 ***Specimen geometry:***

- 391 • The yarns should be positioned symmetrically with respect to the axial midline of the
392 width that should be equal to a multiple of the fabric spacing. The textile should be
393 straight and positioned in the mid-plane of the coupon.
- 394 • The length of the coupons should be adequate to minimize the local effects of the
395 clamping or provide sufficient development length for the fabric in the case of clevis
396 grip. It should be at least greater than the sum of the tabs length plus the extensometer
397 length and double of the specimen width.
- 398 • The coupon geometry must be controlled to verify the straightness and thickness
399 variation. An admissible tolerance must be defined for both quantities. The thickness
400 should be measured in at least five positions along the coupon length.
- 401 • The coupons should not present evident cracks before the test.
- 402 • The differential shrinkage of the two sides of the coupons can cause a curvature that is
403 detrimental for the test because it can cause cracks when the coupon is fixed into the

404 grips of the testing machine. Therefore the planarity of the coupons is very important and
405 must be controlled.

406 ***Gripping:***

- 407 • The choice of the gripping system depends on the final objective of the experimental
408 investigation. If the objective is the characterization (“initial type testing”) of the FRCM
409 system the clamping grips that allow for torsional rotation can provide a complete
410 evaluation of the mechanical properties and all the parameters that characterize the
411 trilinear stress-strain curves can be determined.
- 412 • When the objective is the investigation of the maximum load bearing capacity of the
413 system for the reinforcing application, the clevis type grips are preferred. These are also
414 suggested in the case of on-site acceptance tests of the material and the system.

415 ***Measurements:***

- 416 • Extensometers are ideal to assess the deformations in the coupons. The optimum setup
417 would include four LVDTs placed on the opposite sides of the coupons but it was
418 demonstrated that even a single extensometer with an adequate gauge length provides
419 reliable results. In the literature there are discussions of the ideal measurements
420 [Contamine et al, 2011].

421 **Conclusions**

422 Uniaxial tensile testing of composite material specimens was performed for the main purpose of
423 determining the characteristic mechanical behavior of the material under controlled loading
424 conditions. It is the most accepted method for obtaining material parameters needed for design

425 calculations. The influence of different test set-ups and measurement techniques was presented
426 through the results of an extensive experimental investigation. The selection of the two gripping
427 systems was based on the following considerations. The “clevis grip” is preferred to reproduce
428 the actual behavior that FRCM materials present in the field. With this boundary condition, the
429 tensile behavior was characterized by an initial elastic phase and then a second, lower modulus
430 phase due to cracking of the matrix and slippage between fabric and matrix. The “clamping grip”
431 was selected to obtain a complete characterization of the composite and to produce a tensile
432 failure of each of the constitutive materials of the composite. With this boundary condition, the
433 experimental data confirmed that the behavior of FRCM materials in tension is characterized by
434 trilinear curves. The first part corresponds to the un-cracked phase of the mortar while in the
435 second phase the cracks develop and in the third phase only the fiber reinforcement can carry the
436 applied load. In this phase the measured stiffness and ultimate strength of the specimens
437 correspond to the relevant values of the dry fabrics.

438 A critical analysis was reported regarding the influence of the elongation measurement
439 techniques. Accurate measurements of the deformation behavior of FRCM systems is difficult
440 because elongation measurement instruments are designed to be placed on the exterior surface of
441 specimens, thus capturing only the average deformation experienced by the mortar matrix.
442 Moreover, the deformation through the cross-section of the FRCM is not homogeneous, and the
443 telescopic behavior of the fibers in the yarns cannot be measured with instruments installed on
444 the exterior surface of the material.

445 The investigation of the overlap of the fabric with clevis grips showed that generally, the overlap
446 length must be greater than or equal to the tab length used for load application which itself is a
447 function of the fabric development length within the matrix. This investigation is still in

448 progress, but preliminary tests performed both with clamping grips and clevis grips demonstrate
449 that an overlap of 100 mm is insufficient and must be increased to a minimum of 150 mm.
450 These results highlight the importance for guidelines and recommendations that allow a complete
451 characterization of FRCM composite systems. The two test set-ups investigated in this paper
452 demonstrated the two perspectives involved in the mechanical characterization of the tensile
453 behavior of the material, both, the full capacity of the system and its behavior in field
454 applications.

455 **Acknowledgements**

456 The authors gratefully acknowledge the National Science Foundation (NSF) for the support
457 provided to the Industry/University Center for Integration of Composites into Infrastructure
458 (CICI) under grant no. IIP-0933537 and its industrial members. Any opinions, findings, and
459 conclusions or recommendations expressed in this material are those of the authors and do not
460 necessarily reflect the views of the NSF. Part of the analyses were developed within the activities
461 of Rete dei Laboratori Universitari di Ingegneria Sismica – ReLUIS for the research program
462 funded by the Dipartimento di Protezione Civile – Progetto Esecutivo 2014.

463 **References**

- 464 AC434 (2013). “Acceptance criteria for masonry and concrete strengthening using fiber-
465 reinforced cementitious matrix (FRCM) composite systems.” ICC-Evaluation Service,
466 Whittier, CA.
- 467 ACI (American Concrete Institute). (2013). “Design and construction guide of externally bonded
468 FRCM systems for concrete and masonry repair and strengthening,” *ACI 549.4R-13*,
469 Farmington Hills, MI.

470 Andic-Cakir, O., Sarijanat, M., Tufekci, H.B., Demirci, C., Erdogan, U.H. (2014). "Physical and
471 mechanical properties of randomly oriented coir fiber-cementitious composites."
472 Composites Part B, 61, 49-54.

473 Arboleda, D., Loreto, G., De Luca, A., Nanni, A. (2012). "Material characterization of fiber
474 reinforced cementitious matrix (FRCM) composite laminates." Proc, 10th International
475 Symposium on Ferrocement and Thin Reinforced Cement Composites, Havana, Cuba,
476 29-37.

477 Arboleda, D., Yuan, S., Giancaspro, J., & Nanni, A. (2013). "Comparison of strain measurement
478 techniques for the characterization of brittle, cementitious matrix composites." Research
479 and Applications in Structural Engineering, Mechanics and Computation, Cape Town,
480 South Africa, 1567.

481 Arboleda, D. (2014). "Fabric Reinforced Cementitious Matrix (FRCM) composites for
482 infrastructure strengthening and rehabilitation: characterization methods." Ph.D Thesis.
483 University of Miami, USA.

484 Babaeidarabad, S., Arboleda, D., Loreto, G., Nanni, A. (2014). "Shear strengthening of un-
485 reinforced concrete masonry walls with fabric-reinforced-cementitious-matrix."
486 Construction and Building Materials, 65, 243-253.

487 Banholzer, B., Brockmann, T., Brameshuber, W. (2006). "Material and bonding characteristics
488 for dimensioning and modelling of textile reinforced concrete (TRC) elements."
489 Materials and Structures, 39, 749-763.

490 Bertolesi, E., Carozzi, F.G., Milani, G., Poggi, C. (2014). "Numerical modelling of Fabric
491 Reinforced Cementitious Matrix composites (FRCM) in tension." Construction and
492 Building Materials, 70, 531-548.

493 Bianchi, G., Arboleda, D., Carozzi, F.G., Poggi, C., Nanni, A. (2013). "Fabric Reinforced
494 Cementitious Matrix (FRCM) materials for structural rehabilitation." IAHS 2013: 39th
495 World Congress on Housing Science, Milano, Italy.

496 Bianchi, G., Carozzi, F.G., Poggi, C., Nanni, A. (2014). "Fabric-Reinforced-Cementitious-
497 Matrix (FRCM) per la riabilitazione strutturale: aderenza al supporto." REHABEND
498 2014: Congreso Latinoamericano sobre Patologia de la Construcción, Tecnología de la
499 Rehabilitación y Gestión del Patrimonio, Santander, Spain.

500 Carozzi, F.G., Poggi, C. (2015). "Mechanical properties and debonding strength of Fabric
501 Reinforced Cementitious Matrix (FRCM) systems for masonry strengthening."
502 Composites: Part B, 70, 215-230.

503 Contamine, R., Si Larbi, A., Hamelin, P. (2011). "Contribution to direct tensile testing of textile
504 reinforced concrete (TRC) composites." Material science and engineering: A, 528(29),
505 8589-8598.

506 D'Ambrisi, A., Feo, L., Focacci, F. (2012). "Experimental analysis on bond between PBO-
507 FRCM strengthening materials and concrete." Composites Part B, 44(1), 524-532.

508 De Santis, S., de Felice, G. (2015). "Tensile behavior of mortar-based composites for externally
509 bonded reinforcement systems." Composites: Part B, 68, 401-413.

510 EN 1015-11 (1999). "Methods of test for mortar for masonry - Determination of flexural and
511 compressive strength of hardened mortar." UNI Standard.

512 EN 12390-6 (2009). "Testing hardened concrete - Tensile splitting strength of test specimens."
513 UNI Standard.

514 EN 14580 (2005). "Natural stone test methods - Determination of the static elastic modulus."
515 UNI Standard.

516 EN ISO 10618/2005 (2005). "Carbon Fiber - Determination of tensile properties of resin-
517 impregnated yarn." UNI Standard.

518 Hartig, F., Jesse, F., Schicktanz, K., Haubler-Combe, U. (2012). "Influence of experimental
519 setups on the apparent uniaxial tensile load-bearing capacity of textile reinforced concrete
520 specimens." *Materials and structures*, 45, 433-446.

521 Hartig, J., Jesse, F., Haubler-Combe, U. (2010). "Evaluation of experimental setups for
522 determining the tensile strength of textile reinforced concrete." *International RILEM
523 Conference on Materials Science - MATCI, Aachen, I*, 117-127.

524 Jesse, F., Will, N., Curbach, M., Hegger, J. (2008). "Loadbearing behavior of TRC. 'Textile
525 reinforced concrete'." *American Concrete Institute Special Publication SP 250*,
526 *symposium at the ACI fall convention 2005, November 6-10, Kansas City, Missouri,*
527 *USA / ed.: A. Dubey. Farmington Hills, Mich., ISBN: 978-0-87031-266-3, 978-1-605-*
528 *60366-7, 1-605-60366-X.*

529 Loreto, G., Leardini, L., Arboleda, D., and Nanni, A. (2014). "Performance of RC Slab-Type
530 Elements Strengthened with Fabric-Reinforced Cementitious-Matrix Composites." *J.
531 Compos. Constr.* 18, SPECIAL ISSUE: 10th Anniversary of IIFC, A4013003.

532 Mobasher, B., Peled, A., Pahilajani, J. (2006). "Distributed cracking and stiffness degradation in
533 fabric-cement composites." *Materials and Structures*, 39, 317-331.

534 Molter, M. (2005). "Zum Tragverhalten von textildbewehrtem Beton." PhD thesis, RWTH
535 Aachen.

536 Ombres, L. (2012). "Debonding analysis of reinforced concrete beams strengthened with fiber
537 reinforced cementitious mortar." *Engineering Fracture Mechanics*, 81, 94-109.

538 Orlowsky, J., Raupach, M. (2008). "Durability Model for AR-glass Fibres in Textile Reinforced
539 Concrete." *Materials and Structures*, 41(7), 1225-1233.

540 Papanicolaou, C.G., Triantafillou, T.C., Papathanasiou, M., Karlos, K. (2008). "Textile
541 reinforced mortar (TRM) versus FRP as strengthening material of URM walls: out-of-
542 plane cyclic loading." *Materials and Structures*, 41, 143-157.

543 Papantoniou I.C. and Papanicolaou C.G. (2012), "Flexural Behavior of One-Way Textile
544 Reinforced Concrete (TRC) / Reinforced Concrete (RC) Composite Slabs", Proceedings
545 of the 15th European Conference on Composite Materials - ECCM15, Venice, Italy

546 Peled, A., Zaguri, E., Marom G. (2008). "Bonding characteristics of multifilament polymer yarns
547 and cement matrices." *Composites Part A*, 39, 930-993.

548 Soranakom, C., Mobasher, B. (2009). "Geometrical and mechanical aspects of fabric bonding
549 and pull-out in cement composites." *Materials and Structures*, 42, 765-777.

550 Triantafillou, T. (2012). "Textile-based composite versus FRP as strengthening and seismic
551 retrofitting materials for concrete and masonry structures." *Concrete Repair,*
552 *Rehabilitation and Retrofitting III - Proceedings of the 3rd International Conference on*
553 *Concrete Repair, Rehabilitation and Retrofitting, ICCRRR 2012: 80-88*

554 Zhu, D., Peled, A., Zaguri, E., Mobasher, B. (2011). "Dynamic tensile testing of fabric-cement
555 composites." *Construction and Building Materials*, 25, 385-395.

556

557 **Table of figures**

558 Figure 1. Test set-ups: a) steel plate inside specimen; b) steel flanges; c) clevis (adhesive tension
559 and shear) grips; d) clamping grips

560 Figure 2. Idealized stress-strain curves a) stand-alone fabric, b) clamped FRCM, c) pinned
561 FRCM

562 Figure 3. a) PBO-FRCM system; b) C-FRCM system

563 Figure 4. Fabric geometry: a) PBO; b) glass; c) coated glass; d) carbon; e) coated carbon
564 (dimensions in mm)

565 Figure 5. Tensile test set-up: a) clevis grip; b) clamping grip

566 Figure 6. Differences in strain measurement based on grip type

567 Figure 7. Stress-strain curves with clevis grip of different FRCM materials

568 Figure 8. Stress-strain curves with clamping grip of different FRCM materials

569 Figure 9. PBO-FRCM single layer behavior with the different test setups

570 Figure 10. C-FRCM single layer behavior with the different test setups

571 Figure 11. cC-FRCM: Two-ply vs. one-ply

572 Figure 12. PBO-FRCM lap splice behavior with the different test setups

573

574

575

Table 1 – Mechanical properties of the yarns

Fabric	# yarns	Cross section area [mm²]	# tests	Average stress at failure [GPa]	C.o.V. [%]	Elastic modulus [GPa]	C.o.V. [%]
PBO fiber	1 yarn	0.41	6	3.9	3.2	216	20.8
	4 yarns	1.64	4	3.4	7.3	-	-
C fiber	1 yarn	0.42	3	1.9	14.9	203	9.8
	4 yarns	1.68	3	1.9	10.4	-	-
cC fiber	1 yarn	2.68	3	1.3	9.2	263	11.2
G fiber	1 yarn	0.24	4	1.4	11.4	49	-
cG fiber	1 yarn	0.90	5	1.2	2.7	56	30.5
	3 yarns	2.70	5	1.1	1.3	-	-

576

577

578

Table 2 – Mechanical properties of the matrix

Matrix type	Tensile EN 12390-6		Compressive EN 1015 -11		Flexural EN 1015 -11		Elastic modulus EN 14580 (GPa)
	Strength (MPa)	CoV (%)	Strength (MPa)	CoV (%)	Strength (MPa)	CoV (%)	
Mortar used with PBO fabric	4.75 (7)*	4.05	33.90 (5)	10	> 2 (ds)	-	> 6 (ds)
Mortar used with C fabric	3.30 (5)	3.6	24.02 (5)	2.5	3.5 (ds)	-	> 7 (ds)
Mortar used with cC fabric	3-5 (ei)	-	> 45 (ds)	-	7 (ei)	-	7 (ei)
Mortar used with G fabric	2-4 (ei)	-	10 (ds)	-	3 (ei)	-	5 (ei)
Mortar used with cG fabric	3-5 (ei)	-	27.13 (7)	4.1	8.4 (14)	13.15	8 (ds)

579 **Note: Within brackets # of tested coupons or source of data (ds = data sheet; ei= estimated*
580 *interval)*

581

582

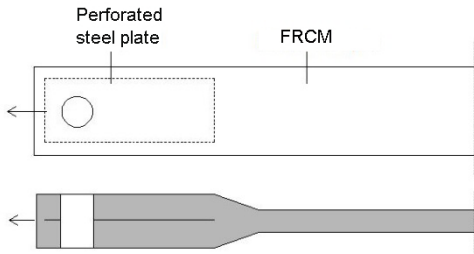
Table 3 – Results of tensile tests

Material	Grip type (#)*	Value type	E ₁ (GPa)	E ₂ (GPa)	E ₃ (GPa)	σ _{t1} (MPa)	σ _{t2} (MPa)	σ _u (MPa)	ε _{t1} (%)	ε _{t2} (%)	ε _u (%)	E* ₁ (GPa)	σ* _{t1} (MPa)
PBO-FRCM 4 yarns	Clevis (10)	Average	1805	128	-	375	-	1664	0.017	-	1.75	-	-
		CoV (%)	25	12	-	22	-	5	25	-	8	-	-
C-FRCM 4 yarns	Clevis (5)	Average	512	80	-	458	-	1031	0.102	-	0.99	-	-
		CoV (%)	25	23	-	10	-	5	44	-	14	-	-
cC-FRCM 3 yarns	Clevis (9)	Average	1570	56	-	381	-	1296	0.023	-	1.64	-	-
		CoV (%)	55	14	-	36	-	12	33	-	14	-	-
cC-FRCM 2-PLY	Clevis (5)	Average	465	52	-	149	-	1133	0.025	-	1.79	8	3
		CoV (%)	24	17	-	24	-	10	37	-	25	15	22
PBO-FRCM 4 yarns	Clamp (34)	Average	1181	76	216	890	1100	3316	0.082	0.5	1.69	5	4
		CoV (%)	20	33	9	15	13	14	31	34	18	20	15
C-FRCM 4 yarns	Clamp (10)	Average	1102	68	186	482	620	1492	0.06	0.24	0.74	5	2
		CoV (%)	18	28	22	21	19	19	13	20	21	18	21
G-FRCM 4 yarns	Clamp (8)	Average	1029	41	56	545	691	1292	0.064	0.44	1.82	2	2
		CoV (%)	31	59	36	25	7	8	25	28	47	31	25
cG-FRCM 3 yarns	Clamp (17)	Average	1310	32	64	460	431	872	0.045	0.38	0.69	6	2
		CoV (%)	33	34	17	30	20	21	41	13	38	34	30

583 *Note: *Within brackets (#) number of tested coupons*

584

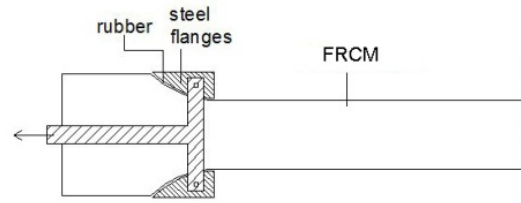
585



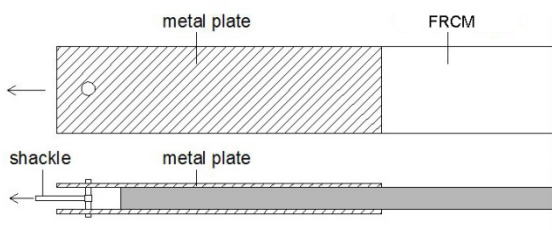
586

587

a)



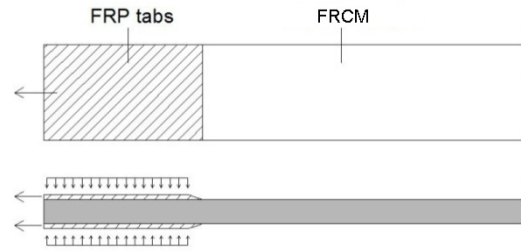
b)



588

589

c)

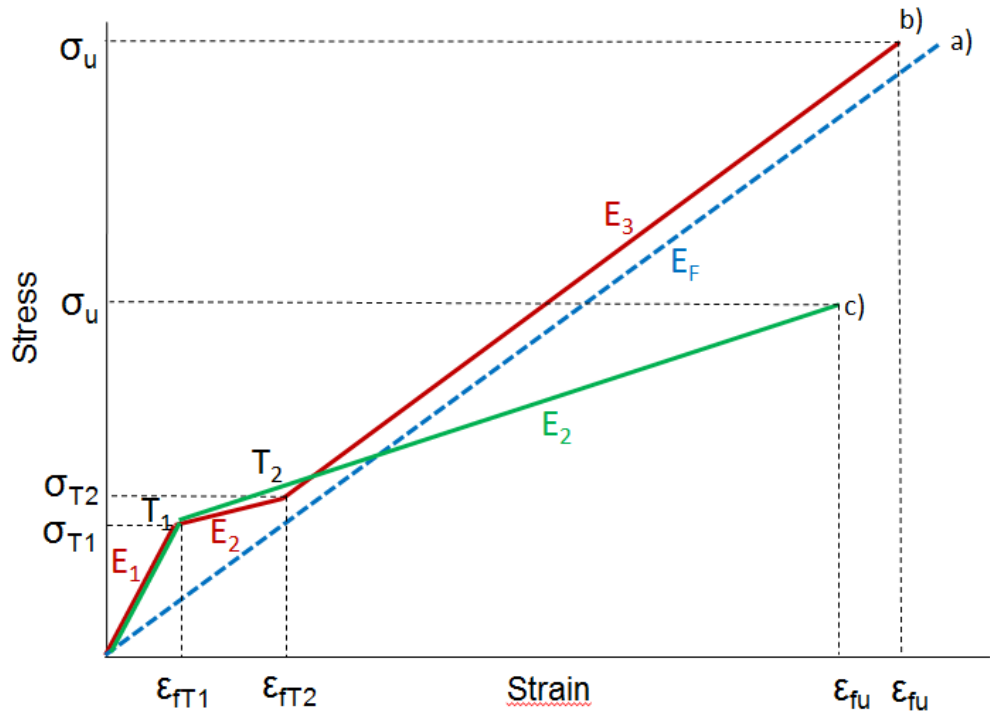


d)

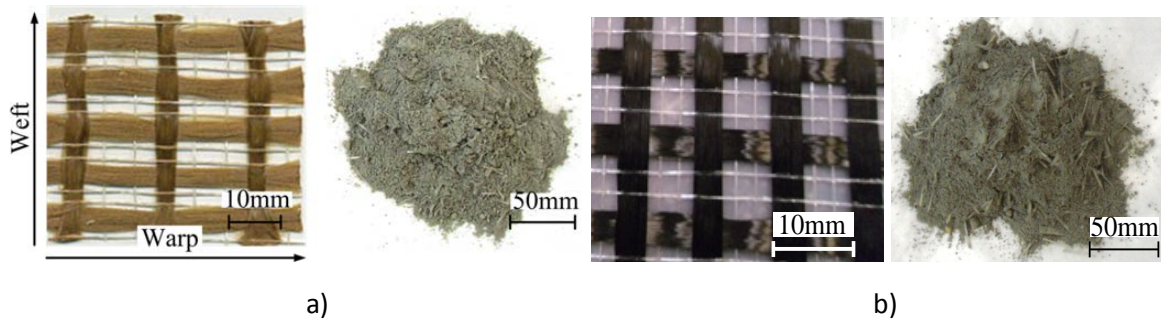
590 Figure 1. Test set-ups: a) steel plate inside specimen; b) steel flanges; c) clevis (adhesive tension
591 and shear) grips; d) clamping grips

592

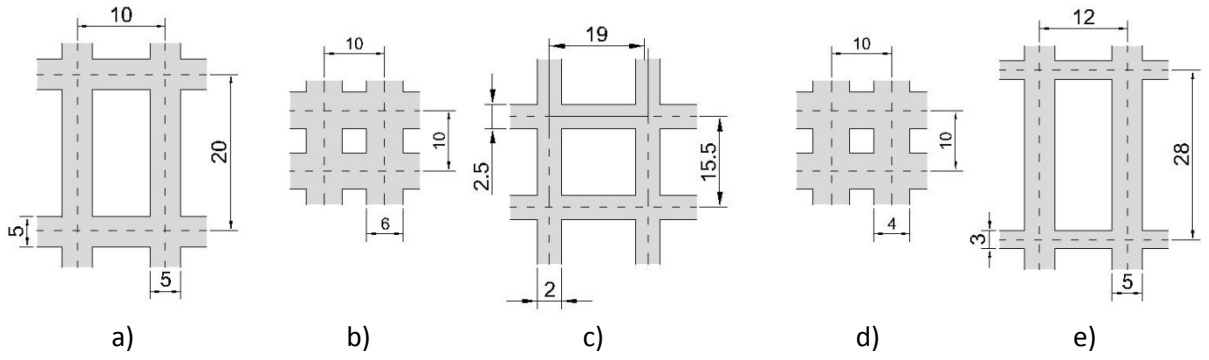
593



594
 595 Figure 2. Idealized stress-strain curves a) stand-alone fabric, b) clamped FRCM, c) pinned FRCM
 596



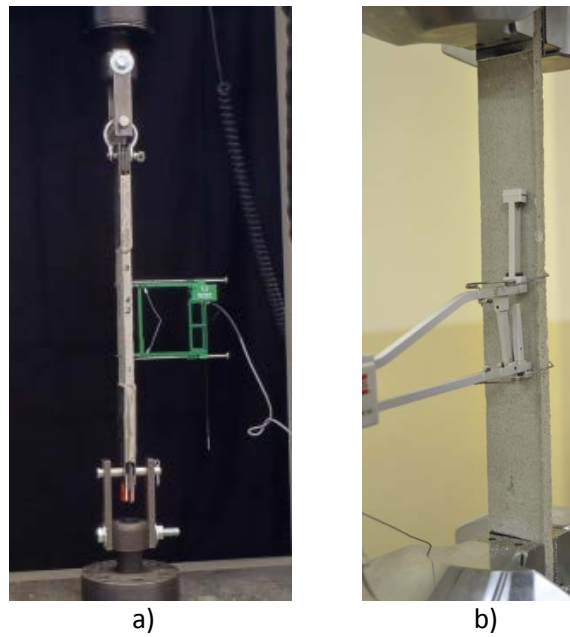
597
 598
 599 Figure 3. a) PBO-FRCM system; b) C-FRCM system
 600



601
602

603 Figure 4. Fabric geometry: a) PBO; b) glass; c) coated glass; d) carbon; e) coated carbon
604 (dimensions in mm)

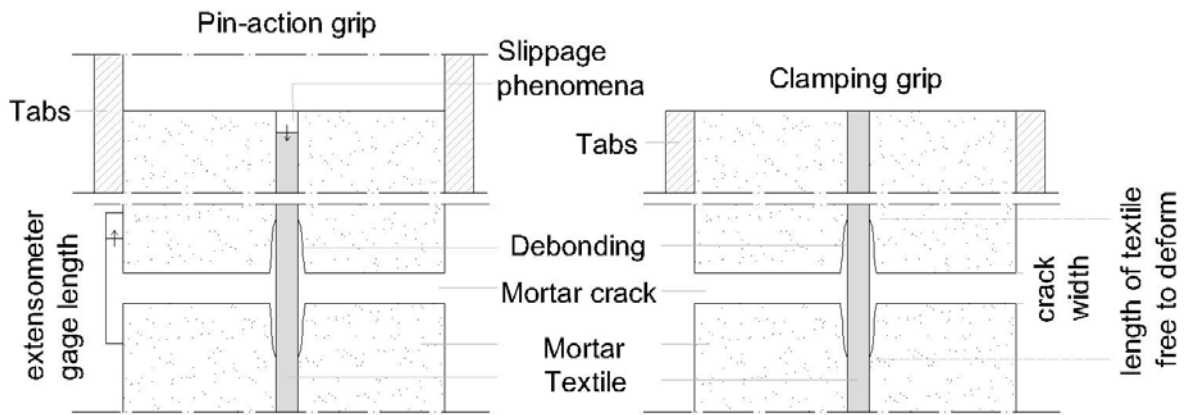
605



606
607

608 Figure 5. Tensile test set-up: a) clevis grip; b) clamping grip
609

610



611

612

613

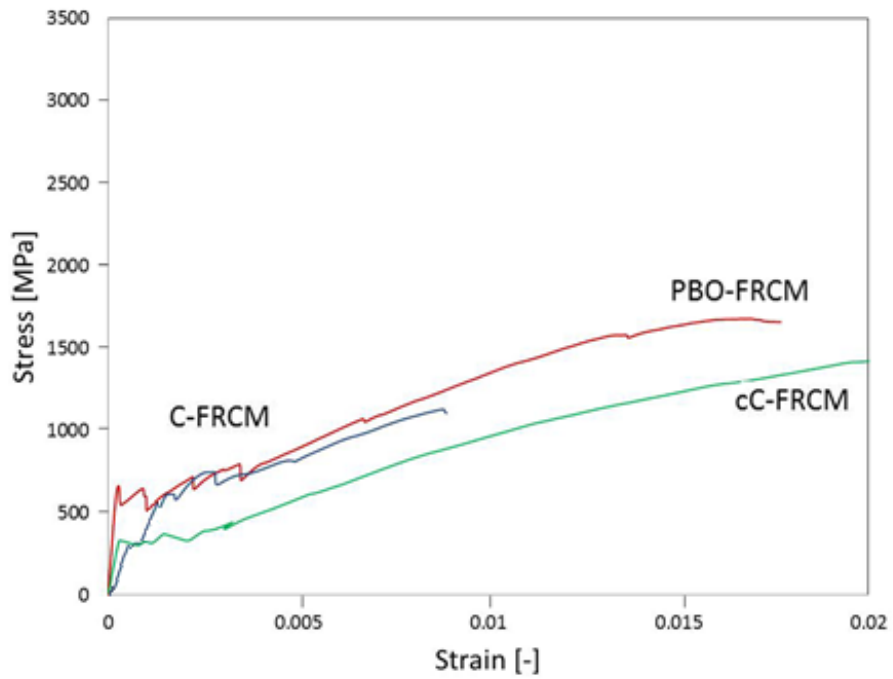
614

615

616

617

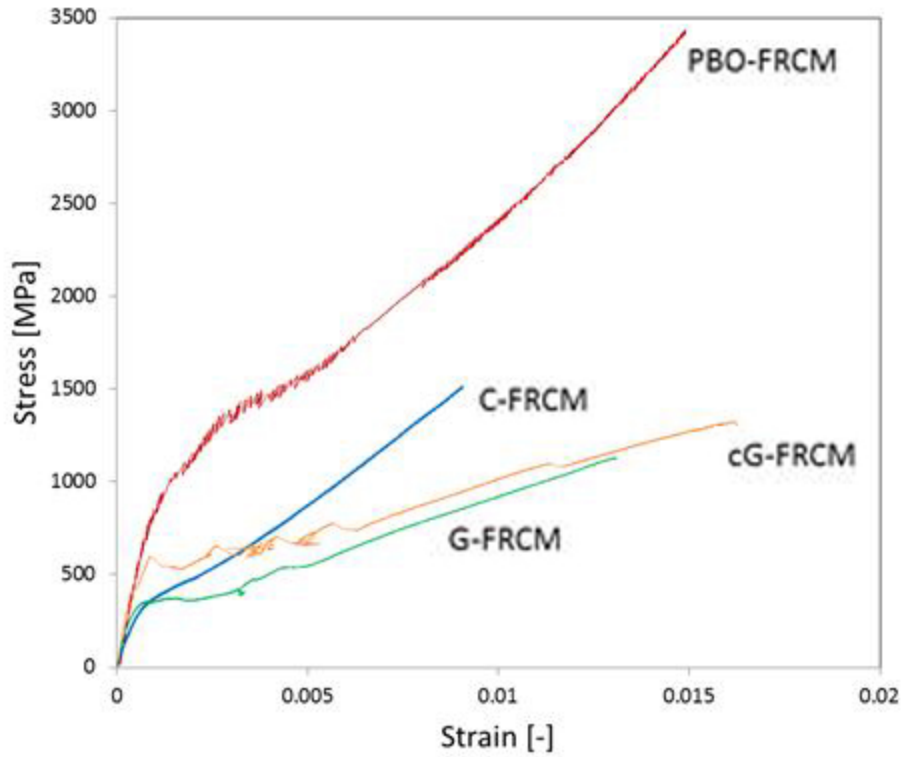
Figure 6. Differences in strain measurement based on grip type



618

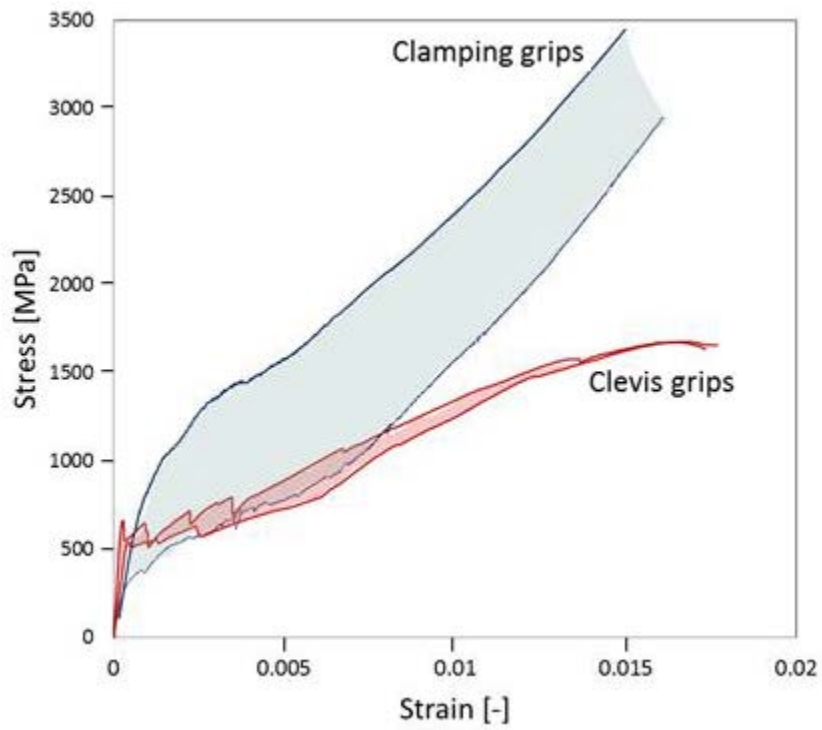
619

Figure 7. Stress-strain curves with clevis grip of different FRCM materials



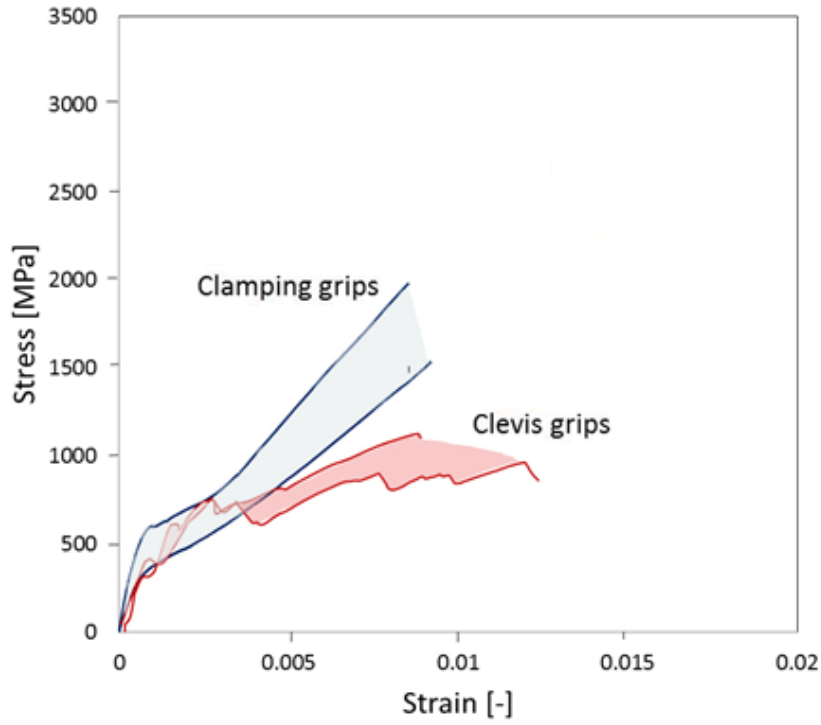
620
621
622

Figure 8. Stress-strain curves with clamping grip of different FRCM materials



623
624

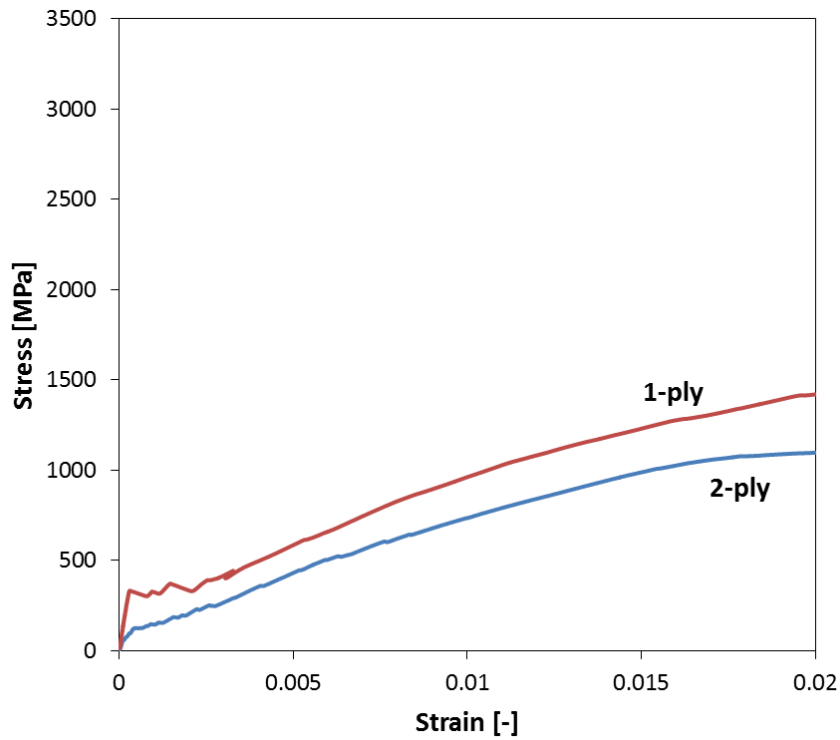
Figure 9. PBO-FRCM single layer behavior with the different test setups



625

626

Figure 10. C-FRCM single layer behavior with the different test setups

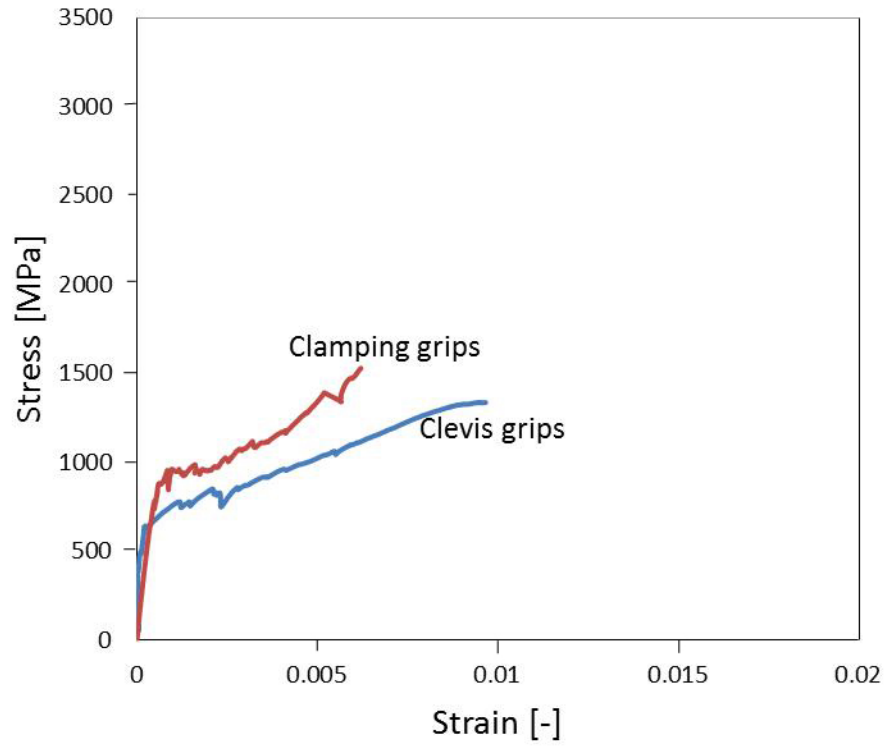


627

628

629

Figure 11. cC-FRCM: Two-ply vs. one-ply



630

631

Figure 12. PBO-FRCM lap splice behavior with the different test setups